

## Comparison of seasonal and spatial variations of leaf area index and fraction of absorbed photosynthetically active radiation from Moderate Resolution Imaging Spectroradiometer (MODIS) and Common Land Model

Y. Tian,<sup>1</sup> R. E. Dickinson,<sup>1</sup> L. Zhou,<sup>1</sup> X. Zeng,<sup>2</sup> Y. Dai,<sup>1</sup> R. B. Myneni,<sup>3</sup> Y. Knyazikhin,<sup>3</sup> X. Zhang,<sup>3</sup> M. Friedl,<sup>3</sup> H. Yu,<sup>1</sup> W. Wu,<sup>1</sup> and M. Shaikh<sup>1</sup>

Received 14 May 2003; revised 31 August 2003; accepted 10 October 2003; published 8 January 2004.

[1] This paper compares by land cover type seasonal and spatial variations of MODIS leaf area index (LAI) and fraction of photosynthetically active radiation (0.4–0.7  $\mu\text{m}$ ) absorbed by vegetation (FPAR) from 2.5 years with those from the Common Land Model (CLM) and investigates possible reasons for notable differences. The FPAR value is mainly determined by LAI in MODIS and both LAI and stem area index (SAI) in CLM. On average, the model underestimates FPAR in the Southern Hemisphere and overestimates FPAR over most areas in the Northern Hemisphere compared to MODIS observations during all seasons except northern middle latitude summer. Such overestimation is most significant in winter over northern high latitudes. The MODIS LAI is generally consistent with the model during the snow-free periods but may be underestimated in the presence of snow, especially for evergreen trees. The positive FPAR bias is mainly attributed to CLM SAI of deciduous canopy and higher LAI than MODIS for evergreen canopy as well. The negative FPAR bias results from several factors, including differences in LAI and soil albedo between CLM and MODIS or limitations of the geometric optics scheme used in the model. Therefore the MODIS algorithm needs to better represent the winter LAI retrievals, while the model needs to better quantify LAI and SAI. Since stems will not have the same single-scattering albedo as green leaves, it may be inappropriate for the model to treat LAI and SAI the same in the FPAR and albedo parameterizations. If so, the role of SAI in these parameterizations needs reformulation. **INDEX TERMS:** 1620 Global Change: Climate dynamics (3309); 1640 Global Change: Remote sensing; 3307 Meteorology and Atmospheric Dynamics: Boundary layer processes; 3322 Meteorology and Atmospheric Dynamics: Land/atmosphere interactions; **KEYWORDS:** LAI, FPAR, MODIS, Common Land Model

**Citation:** Tian, Y., et al. (2004), Comparison of seasonal and spatial variations of leaf area index and fraction of absorbed photosynthetically active radiation from Moderate Resolution Imaging Spectroradiometer (MODIS) and Common Land Model, *J. Geophys. Res.*, 109, D01103, doi:10.1029/2003JD003777.

### 1. Introduction

[2] The land component of climate models represents many processes that control exchanges of energy, momentum and materials between soil, vegetation and the atmosphere, and has long been recognized as important for weather forecasting and climate change [e.g., Dickinson, 1983; Bonan, 1996, 1998; Sellers et al., 1997]. The leaf area

index (LAI) and fraction of photosynthetically active radiation (0.4–0.7  $\mu\text{m}$ ) absorbed by vegetation (FPAR) are identified as two key parameters in the land surface models and are related to albedo, fractional vegetation, and roughness length [Dickinson et al., 1993; Chen and Cihlar, 1996; Bonan, 1996, 1998; Sellers et al., 1997; Myneni et al., 2002; Zeng et al., 2002]. LAI is defined as the one sided green leaf area per unit ground area for broadleaf canopies or the projected needleleaf area for coniferous canopies. Models require LAI as input and compute FPAR from LAI and vegetation albedo to obtain transpiration. The model values of LAI and FPAR have not previously had reliable observations to be checked against.

[3] Good descriptions of the climatological LAI and FPAR require data over a long period of time and from every region of the terrestrial surface. Satellite remote sensing products can best provide such global fields on a

<sup>1</sup>School of Earth and Atmospheric Sciences, Georgia Institute of Technology, Atlanta, Georgia, USA.

<sup>2</sup>Institute of Atmospheric Physics, University of Arizona, Tucson, Arizona, USA.

<sup>3</sup>Department of Geography, Boston University, Boston, Massachusetts, USA.

regular basis and thus help modelers improve descriptions of land-atmosphere interactions [Henderson-Sellers and Wilson, 1983; Buermann et al., 2001; Zeng et al., 2002]. The launch of TERRA with Moderate Resolution Imaging Spectroradiometer (MODIS) onboard began a new era, by providing for the first time high-quality LAI and FPAR products from MODIS-measured canopy reflectance data [Knyazikhin et al., 1998a, 1998b; Myneni et al., 2002].

[4] Comparison between model-generated and satellite-derived fields reveals discrepancies that suggest possible improvements to both. This study compares the seasonal and spatial variations of MODIS LAI and FPAR, as observed in 2000, 2001 and 2003, with those from the Common Land Model (CLM). It investigates possible reasons for major differences and provides guidance toward improving the model's LAI description and FPAR parameterization. Section 2 describes how LAI and FPAR are computed from CLM and MODIS. Section 3 analyzes seasonal and spatial variations of MODIS LAI and FPAR. Section 4 compares LAI and FPAR between MODIS and CLM, followed by discussion in section 5 and conclusions in section 6.

## 2. LAI and FPAR From MODIS and CLM

### 2.1. MODIS LAI and FPAR

[5] The MODIS LAI-FPAR algorithm is based on three-dimensional radiative transfer theory [Myneni et al., 2002], and developed for inversion using a look-up table (LUT) approach [Knyazikhin et al., 1998a, 1998b; Privette et al., 2002]. The algorithm employs a 1 km land cover map of six major biomes produced from MODIS. The structural characters among these biomes, such as the horizontal (homogeneous vs. heterogeneous) and vertical (single- vs. multistory) dimensions, canopy height, leaf type, soil brightness and climate (precipitation and temperature), are used to define unique model configurations, including some fixed parameter values appropriate for the biome characteristics [Myneni et al., 1997; Privette et al., 2002]. LUTs are then generated for each biome by running the model for various combinations of LAI and soil type. The algorithm ingests atmospherically corrected bidirectional reflectance factors, their uncertainties and corresponding sun-view geometries. It compares the observed reflectances to comparable values evaluated from model-based entries stored in LUTs and derives the distribution of all possible solutions, i.e., LAI and FPAR distribution functions. The standard archived product is the mean of the distribution functions [Knyazikhin et al., 1998a; Myneni et al., 2002]. When this method fails to identify a solution, a back-up method based on relations between the normalized difference vegetation index (NDVI) and LAI and FPAR [Myneni et al., 1997; Knyazikhin et al., 1998a] is used.

[6] The current MODIS 1-km LAI-FPAR product is retrieved from the reflectances of two bands (648 and 858 nm) and on an 8-day compositing period. The product also includes extensive quality control (QC) information regarding cloud and data processing conditions. During each 8-day period, the highest-quality LAI and FPAR are selected (R. B. Myneni et al., MODIS LAI/FPAR product user's guide, 2003, available at ftp://crsa.bu.edu/pub/rmyneni/myneniproduts/MODIS/readme.txt). These data

are further composited over 4 (or 3) consecutive 8-day periods to produce monthly data (Myneni et al., 2003, ftp://crsa.bu.edu/pub/rmyneni/myneniproduts/MODIS/readme.txt). This study uses two and half years of MODIS LAI and FPAR products (MOD15A2, Collection 4) in 2000, 2001, and January through June in 2003. To minimize cloud contamination, the 2.5-year data are further composited to produce a climatology of monthly LAI and FPAR with the best quality, which is used to compare with CLM values.

### 2.2. CLM LAI and FPAR

#### 2.2.1. CLM

[7] The CLM is a recently developed state-of-the-art land surface model, described in detail by Zeng et al. [2002] and Dai et al. [2003]. It has one vegetation layer, 10 unevenly spaced vertical soil layers, and up to 5 snow layers. In this version, every surface grid ( $2.8^\circ \times 2.8^\circ$ ) is subdivided into up to 5 tiles, each tile containing a single land cover type. Zeng et al. [2002] used 16 land cover types based on the IGBP land cover classification and defined a special class type 18 (purely bare soil). Surface input data required for each grid include the central location, soil color type, sand and clay fraction, land cover type and its fraction for each tile. Each vegetation type is assigned a set of time-invariant parameters: optical properties (canopy albedo), morphological properties (canopy roughness, canopy zero plane displacement, inverse square root of leaf dimension, root fraction), and physiological properties. Time-variant parameters include LAI and stem area index (SAI).

#### 2.2.2. LAI and SAI

[8] The monthly LAI climatology used in CLM was derived from the advanced very high resolution radiometers (AVHRR) 8-km NDVI data set from July 1981 to June 1991 [Zeng et al., 2002]. Within each  $10^\circ$ -latitude zone, an annual cycle of LAI for each IGBP land cover type was specified. Since satellite-derived LAIs are defined with respect to unit ground area, they were then divided by the fraction of vegetation [Zeng et al., 2000] to produce green LAI with respect to vegetated area only (denoted as  $L_{AI}$ ) as an input data set for the mosaic treatment of subgrid vegetation variation in the model. Since snow and cloud significantly affect satellite-derived LAI, winter  $L_{AI}$  values were adjusted by

$$L_{AI} = \max(L_{AI}, cL_{AI,max}), \quad (1)$$

for evergreen needleleaf forests ( $c = 0.7$ ) and evergreen broadleaf forests ( $c = 0.8$ ).  $L_{AI,max}$  is the maximum monthly  $L_{AI}$  [Zeng et al., 2002].

[9] Stems and dead leaves are represented by the SAI but its values are poorly known. Zeng et al. [2002] assigned a SAI value that increases from its minimum value in winter to its maximum value in fall for each land cover type and with respect to vegetated areas (denoted as  $S_{AI}$ ) of each  $10^\circ$ -latitude zone. The  $S_{AI}$  value for deciduous broadleaf forests is about 1.0 for most months over most of the latitudinal zones, but increases north of  $30^\circ N$  during and after September, typically adding as much as 2 at its peak in October or November to represent dead leaves.

[10] For each tile,  $L_{AI}$  and  $S_{AI}$  are combined together as leaf and stem area index (denoted as  $L_{SAI}$ ) to calculate

vegetation albedo and FPAR in CLM. Note  $L_{SAI} = L_{AI} + S_{AI}$ .

### 2.2.3. FPAR

[11] This paper determines FPAR at each vegetation tile in CLM by

$$FPAR_v = \frac{I_b + I_d}{S_{v,b}^\downarrow + S_{v,d}^\downarrow}, \quad (2)$$

where  $I_b$  ( $I_d$ ) is the direct (diffuse) solar radiation absorbed by canopy in the visible band (VIS,  $<0.7 \mu\text{m}$ ),  $S_{v,b}^\downarrow$  ( $S_{v,d}^\downarrow$ ) is the direct (diffuse) incident solar radiation at the top of the canopy in VIS, the subscripts  $v$  refer to vegetation, and

$$I_b = (1 - \alpha_{v,b})S_{v,b}^\downarrow \times [1 - \exp(-k_b L_{SAI})], \quad (3a)$$

$$I_d = (1 - \alpha_{v,d})S_{v,d}^\downarrow \times [1 - \exp(-k_d L_{SAI})]. \quad (3b)$$

Variables  $\alpha_{v,b}$  and  $\alpha_{v,d}$  are the direct and diffuse vegetation albedos,  $k_b$  ( $k_b = \frac{G(\mu)}{\mu} \sqrt{1 - \omega}$ ) and  $k_d$  ( $k_d = \sqrt{1 - \omega}$ ) are the PAR extinction coefficient respectively for the direct and diffuse beam solar radiation (time-mean radiation-weighted value);  $G(\mu)$  is the cosine of the angle between the leaf normal and the direction of solar beam and is set as 0.5 in the model;  $\mu$  is cosine of solar zenith angle (SZA);  $\omega$  is the leaf-scattering coefficient (single-scattering albedo) for PAR and is set to 0.15 (Y. Dai et al., The Common Land Model: Documentation and user's guide, 2001, available at <http://climate.eas.gatech.edu/dai/clmdoc.pdf>).

[12] Vegetation albedos in equation (3) are calculated from a geometric optics scheme, which combines canopy and its underlying surface albedos,

$$\alpha_{v,b} = \alpha_c \left[ 1 - \exp\left(-\frac{\omega\beta L_{SAI}}{\mu\alpha_c}\right) \right] + \alpha_g \exp\left[-\left(1 + \frac{0.5}{\mu}\right)L_{SAI}\right], \quad (4a)$$

$$\alpha_{v,d} = \alpha_c \left[ 1 - \exp\left(-\frac{2\omega\beta L_{SAI}}{\alpha_c}\right) \right] + \alpha_g \exp(-2L_{SAI}), \quad (4b)$$

where  $\alpha_c$  is canopy albedo,  $\alpha_g$  is the underlying surface albedo, and the subscripts,  $b$  and  $d$  refer to direct and diffuse beam, respectively. The product  $\omega\beta$  is the upward scattered fraction (CLM sets  $\beta = 0.5$ ). This scheme assumes that vegetation albedo approaches that of the underlying surface,  $\alpha_g$ , when  $L_{SAI}$  goes to zero and approaches a prescribed canopy albedo value,  $\alpha_c$ , when  $L_{SAI}$  goes to its maximum value. The prescribed canopy albedos for each land cover type were inferred initially from the biosphere-atmosphere transfer scheme (BATS) [Dickinson et al., 1993] and then adjusted on the basis of AVHRR-derived albedo data [Zeng et al., 2002].

[13] The underlying bare soil albedo varies with soil color and moisture [Dickinson et al., 1993]:

$$\alpha_g = \alpha_{sat} + \min\{\alpha_{sat}, \max[0.01(11 - 400), 0]\}, \quad (5)$$

where  $\alpha_{sat}$  is saturated soil albedo,  $\theta$  is the ratio of surface soil water volumetric content over its saturated value. CLM

uses prescribed  $\alpha_{sat}$  for 8 soil color types globally from dark to light.

[14] Albedos for the snow covered part of vegetation and underlying surface are re-calculated based on snow albedo. The latter depends on SZA and snow age, and how the latter decreases with time due to growth of snow grain size and accumulation of dirt and soot [Wiscombe and Warren, 1980; Dickinson et al., 1993].

### 2.3. Factors Determining FPAR in CLM

[15] The primary factor determining FPAR in CLM is the  $L_{SAI}$  and canopy albedo. However, it also depends to some extent on SZA and the ratio of direct to total incident solar radiation (FDIR). The MODIS data stream currently does not provide this ratio and the TOA reflectances are converted to surface reflectances assuming the later sees only a direct beam solar flux. Thus the MODIS algorithm assumes FPAR only for direct beam. The dependence of FPAR on SZA and diffuse radiation can be minimized by sampling the CLM output at local 10:30 am. The CLM FPAR also is decreased a small amount by its dependence on underlying soil albedo when  $L_{SAI}$  is small according to equation (3), because of its dependence on  $\alpha_{v,b}$  and  $\alpha_{v,d}$ . This contribution is small and appears to be an artifact of equation (3) making use of  $\alpha_{v,b}$  and  $\alpha_{v,d}$  when use of only the canopy term would be more plausible. We estimate that FPAR should actually be increased by at most a few percent because of canopy absorption of solar radiation reflected by the soil. Such dependency on soil albedo is small compared to other contributions to FPAR and will be discussed in section 5.

[16] Because CLM and MODIS have been shown to be in good agreement with regard to canopy albedo [Zhou et al., 2003], their FPARs are expected to differ primarily due to differences in  $L_{SAI}$  as now addressed. Figure 1 illustrates how a FPAR bias will be given by a  $L_{SAI}$  bias for evergreen broadleaf forests with four  $L_{SAI}$  values, 0.5, 2.0, 4.0 and 6.0. The parameters used include: (1) canopy albedo, 0.04, (2) FDIR, 1.0, and (3) SZA, 0, 20, 40, 60, and 80. Evidently, an overestimation of 1 in  $L_{SAI}$  results in an overestimation of 0.25, 0.1, 0.05 and 0.02 in FPAR for  $L_{SAI} = 0.5, 2.0, 4.0$  and  $6.0$ , respectively, when SZA is 0. For the same  $L_{SAI}$  bias, the smaller the  $L_{SAI}$  value the larger the FPAR bias; and the FPAR bias is more sensitive to a negative  $L_{SAI}$  bias than to a positive bias.

[17] Figure 2 shows how the FPAR- $L_{SAI}$  relationship depends on SZA for evergreen broadleaf forests and open shrublands when FDIR is 1.0 (direct beam only). Evidently, FPAR increases nonlinearly with  $L_{SAI}$ , with the largest rate for the smaller  $L_{SAI}$ . For a given  $L_{SAI}$ , FPAR increases as SZA increases, indicating that a more efficient photosynthesis occurs during the morning and afternoon than at noontime due to the longer path of sunlight traveling within the canopy at larger SZA. The FPAR value of evergreen broadleaf forests is larger than that of open shrublands, resulting from differences in their prescribed canopy albedos, 0.04 for the former versus 0.14 for the latter.

[18] FPAR also depends on FDIR. Figure 3 illustrates that this dependence is (1) strongest for an  $L_{SAI}$  from 0.5 to 1.5 and relatively small for an  $L_{SAI}$  greater than 4 and (2) largest

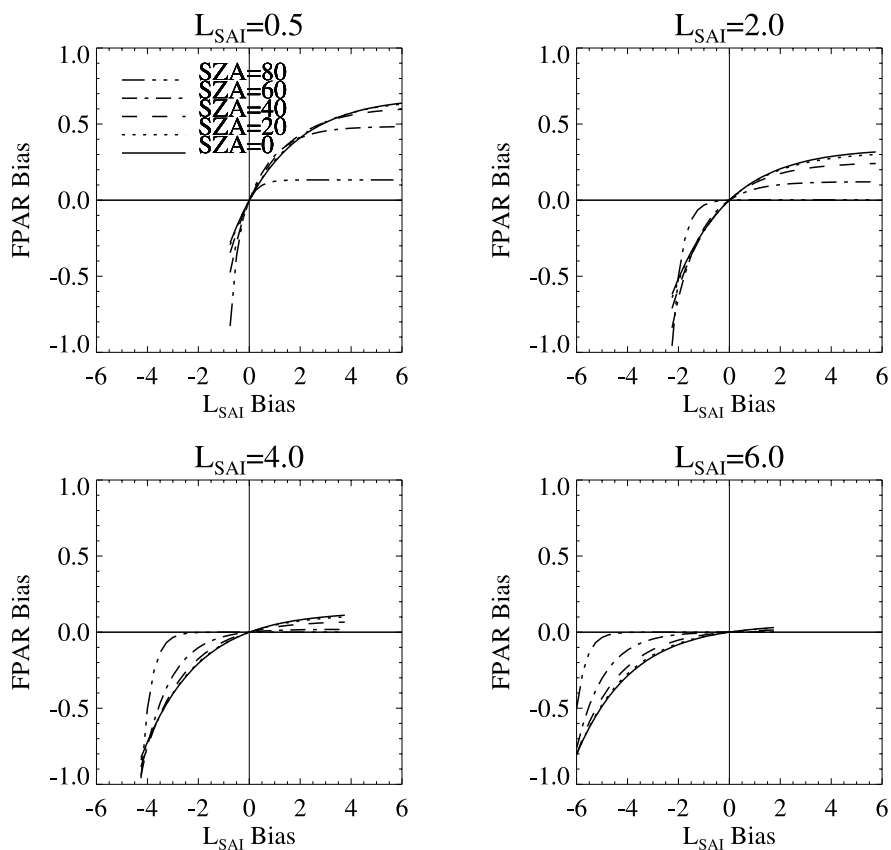


**Figure 1.** FPAR bias versus  $L_{SAI}$  bias relationship simulated from equation (2) for evergreen broadleaf forests with four  $L_{SAI}$  values, 0.5, 2, 4, and 6, at SZA = 0, 20, 40, 60, and 80. Canopy albedo is set as 0.04 and the ratio of direct to total incident solar radiation (FDIR) is set as 1.0.

for a SZA that is near overhead or near the horizon and smallest for SZA near  $60^\circ$ .

### 3. Seasonal and Spatial Variations in MODIS LAI and FPAR

[19] Global distributions of MODIS LAI and FPAR for March and July, corresponding to winter and summer,

are shown in Figure 4 at the model resolution. Late winter (March) is chosen to stay away from mid-winter (January) at which time there is much more snow and too little sun to provide much energy either for the land surface or for remote sensing in high latitudes. The LAI and FPAR values peak during local summer (wet season). The two hemispheres clearly show opposite seasonality.

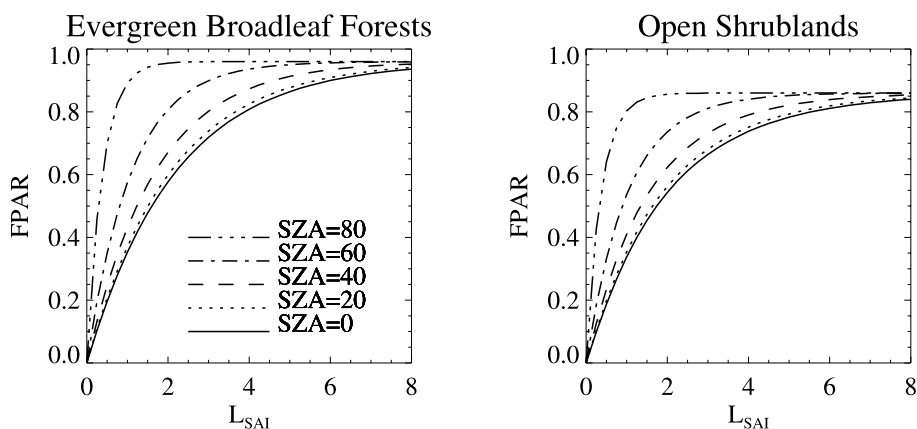


**Figure 2.** FPAR- $L_{SAI}$  relationship simulated from equation (2) at SZA = 0, 20, 40, 60, and 80 for evergreen broadleaf forests and open shrublands when FDIR is 1.0.

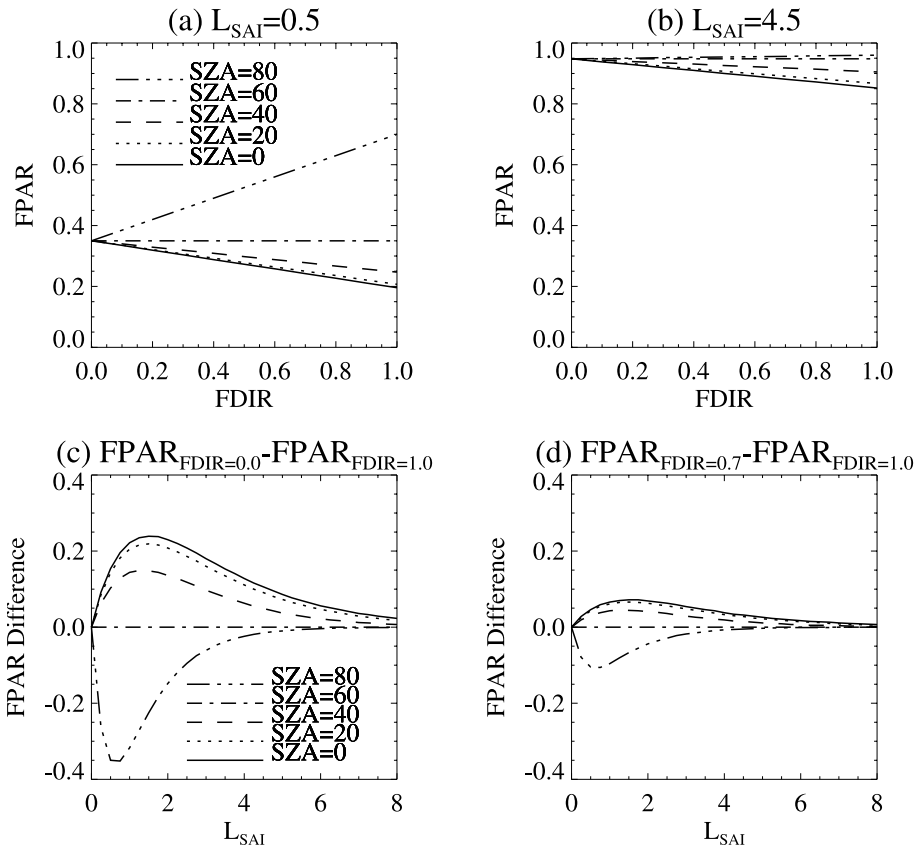


**Figure 3.** FPAR-FDIR relationship at  $SZA = 0, 20, 40, 60,$  and  $80$  for (a)  $L_{SAI} = 0.5$  and (b)  $L_{SAI} = 4.5$  and FPAR difference in (c)  $FPAR_{FDIR=0.0} - FPAR_{FDIR=1.0}$  and (d)  $FPAR_{FDIR=0.7} - FPAR_{FDIR=1.0}$  as a function of  $L_{SAI}$  at  $SZA = 0, 20, 40, 60,$  and  $80$ , simulated from equation (2).

[20] To analyze LAI and FPAR latitudinal variations, we used the MODIS IGBP land cover classification map [Friedl *et al.*, 2002] to spatially aggregate all 1 km MODIS pixels into  $10^\circ$  latitudinal bands. In each band, monthly mean LAI and FPAR are calculated for each land cover type. Here we only show results for 5 typical vegetation types (Figure 5): evergreen needleleaf forests (class 1), evergreen broadleaf forests (class 2), deciduous needleleaf forests (class 3), deciduous broadleaf forests (class 4), and savannas (class 9). These classes are then divided into group 1 (classes 1, 3 and 4) and group 2 (classes 2 and 9).

[21] The LAI (FPAR) values for group 1 increase dramatically from winter to summer and maximize around 4.5 (0.9). For each class, large differences between latitudinal bands are seen in all seasons except summer. The winter LAI and FPAR values for class 1 are surprisingly low in high latitudes ( $55^\circ N - 65^\circ N$ ) as discussed in sections 4.2 and 5.

[22] The classes of group 2 are mainly located at tropical regions ( $25^\circ S - 25^\circ N$ ). The seasonality of savannas differs between the two hemispheres. The Northern Hemisphere (NH) and Southern Hemisphere (SH) LAI peak around March and September, respectively. Unlike savannas, evergreen broadleaf forests in  $15^\circ S - 5^\circ N$  display an indistinct seasonal cycle with phase of precipitation.

[23] Seasonal variations of FPAR follow those of LAI for all classes. FPAR varies little for  $LAI > 3$  but more for  $LAI < 3$  among latitudinal bands. The FPAR is nearly linear with

LAI variation for low LAI values but varies little for high LAI values, as illustrated in Figure 2.

#### 4. Comparison of LAI and FPAR Between MODIS and CLM

[24] We performed an 11-year simulation of CLM coupled with the NCAR CCM3, a spectral atmospheric model with resolution at about  $2.8^\circ \times 2.8^\circ$  and 18 vertical levels [Kiehl *et al.*, 1998], with climatological sea surface temperatures (SSTs). The FPAR values from the last year were used to compare with MODIS observations while the first 10-year run was used as a spinup. The prescribed LAI in CLM varies monthly but keeps constant with years. To make the comparison more precise, FPAR at local time 10:30am was sampled each day from CLM and the mean value was chosen over each month.

[25] Because  $L_{AI}$ ,  $S_{AI}$ , and FPAR in CLM are defined with respect to vegetated area only, we converted them into values per unit ground area (denoted as LAI and SAI in this paper) for comparison with those of MODIS. Note MODIS FPAR is calculated based on only LAI while CLM treats both LAI and SAI the same and uses  $L_{SAI}$  ( $L_{SAI} = LAI + SAI$ ) to calculate FPAR.

##### 4.1. Spatial Patterns of Difference at Global Scale

[26] Global distributions of differences between CLM  $L_{SAI}$  and FPAR and MODIS LAI and FPAR in March

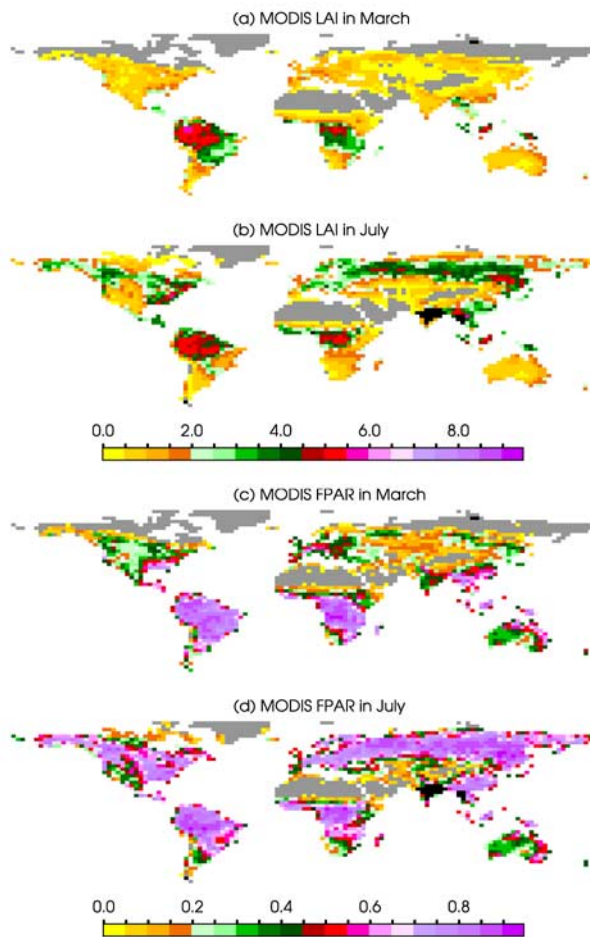


**Figure 4.** Spatial pattern of MODIS LAI in (a) March and (b) July and MODIS FPAR in (c) March and (d) July. Areas in black denote no data.

and July are shown in Figure 6. For simplicity, the model LSAI is also referred to as LAI in this section. On an average, CLM values are consistent with those of MODIS in spatial distribution and in rough agreement with the magnitude. Here we mainly focus on notable differences in LAI and FPAR.

[27] In March, CLM values are lower by about 0.5–1.5 for LAI and 0.05–0.25 for FPAR than is observed over most areas in the SH except southwest Australia. Over most regions in the NH, CLM gives higher values than MODIS, especially at high latitudes where the differences can reach 2 for LAI and 0.5 for FPAR. A relatively large difference occurs in  $5^{\circ}\text{N}$ – $15^{\circ}\text{N}$  over the African continent, where savannas and woody savannas are located. Over southeast Asia and western Europe, where croplands or vegetation mosaics were classified by both CLM and MODIS, CLM values are slightly lower than observations. In July, the LAI and FPAR differences remain similar in the spatial pattern globally as those in March but with a much smaller magnitude over most regions except a small negative bias over areas in central USA, boreal Eurasia, and southeast Asia.

[28] To better illustrate spatial and seasonal variations of the LAI and FPAR differences globally, we calculated their monthly means within each  $5.6^{\circ}$  latitudinal zone (Figure 7). The difference remains negative throughout the whole year

in the SH, with a magnitude slightly larger during local summer than winter. In the NH, the positive discrepancy gradually changes to the negative in  $15^{\circ}$ – $45^{\circ}\text{N}$  and becomes smaller beyond  $45^{\circ}\text{N}$  from winter to summer.

[29] The positive FPAR bias generally corresponds to the positive LAI bias and vice versa, especially over northern high latitudes where the largest bias is observed, indicating that the former can be mainly explained by the latter, as shown in Figure 1. For areas where the LAI bias is not significant, other variables could also contribute to the FPAR bias. For example, the negative FPAR difference is much larger in the spatial pattern than the LAI difference over some areas in northern middle latitudes. Possible reasons are discussed in section 5.

## 4.2. Seasonal Variation at Regional Scale

[30] We chose 6 land cover types to examine seasonal variations of LAI and FPAR in CLM and MODIS. For each land cover, a group of model grids, defined by the same dominant land cover type in both CLM and MODIS, is selected and averaged based on their geographical locations.

### 4.2.1. Deciduous Needleleaf Forests

[31] The region in Siberia ( $50^{\circ}$ – $65^{\circ}\text{N}$ ,  $100^{\circ}$ – $140^{\circ}\text{E}$ ) was chosen because deciduous needleleaf forests are without leaves during winter (Figure 8). CLM shows significant higher FPAR values in winter than those from MODIS but comparable values in summer. Since CLM and MODIS have a consistent LAI seasonal cycle, the nearly constant SAI of about 1 in CLM should be mainly responsible for the FPAR bias. Such SAI could lead to the observed significantly higher FPAR in winter as shown in Figure 1. Therefore, for deciduous trees the winter FPAR bias mainly results from the model SAI. Figure 9 shows seasonal variations of CLM  $L_{\text{AI}}$  and  $S_{\text{AI}}$  (with respect to vegetated area) in  $50^{\circ}$ – $59^{\circ}\text{N}$  for four deciduous vegetation types. Evidently,  $S_{\text{AI}}$  is always higher than  $L_{\text{AI}}$  during winter. This explains why CLM has much higher LSAI and FPAR than MODIS in middle and high latitudes during NH winter.

[32] SAI is an important canopy property in land surface models. The presence of SAI during winter could decrease snow albedo through its absorption and consequent reduction in openings exposed to sun and increase in shadow. MODIS does not provide SAI values; therefore we could not evaluate their accuracy in the model. CLM treats LAI and SAI the same in calculating FPAR, which makes the contribution of SAI to FPAR much larger than that of LAI in winter. However, branches and dead leaves should have very limited or no photosynthesis. Comparison of albedo between MODIS and CLM [Zhou *et al.*, 2003] also suggests that CLM significantly underestimates winter albedo in the presence of snow in high latitudes due to its high LSAI.

### 4.2.2. Evergreen Needleleaf Forests

[33] The region in North America ( $40^{\circ}$ – $60^{\circ}\text{N}$ ,  $130^{\circ}$ – $60^{\circ}\text{W}$ ) is chosen (Figure 10). Like Figure 8, CLM gives higher FPAR in winter, mainly due to the model SAI. The higher winter LAI in CLM may also contribute. Contrary to reality for evergreen trees, MODIS LAI approaches zero in winter, suggesting that MODIS may give too small winter LAI due to snow effects (more discussion in section 5).

### 4.2.3. Open Shrublands

[34] We selected two regions (Figure 11), one in high latitude ( $55^{\circ}$ – $70^{\circ}\text{N}$ ,  $170^{\circ}\text{W}$ – $170^{\circ}\text{E}$ ) and the other in low

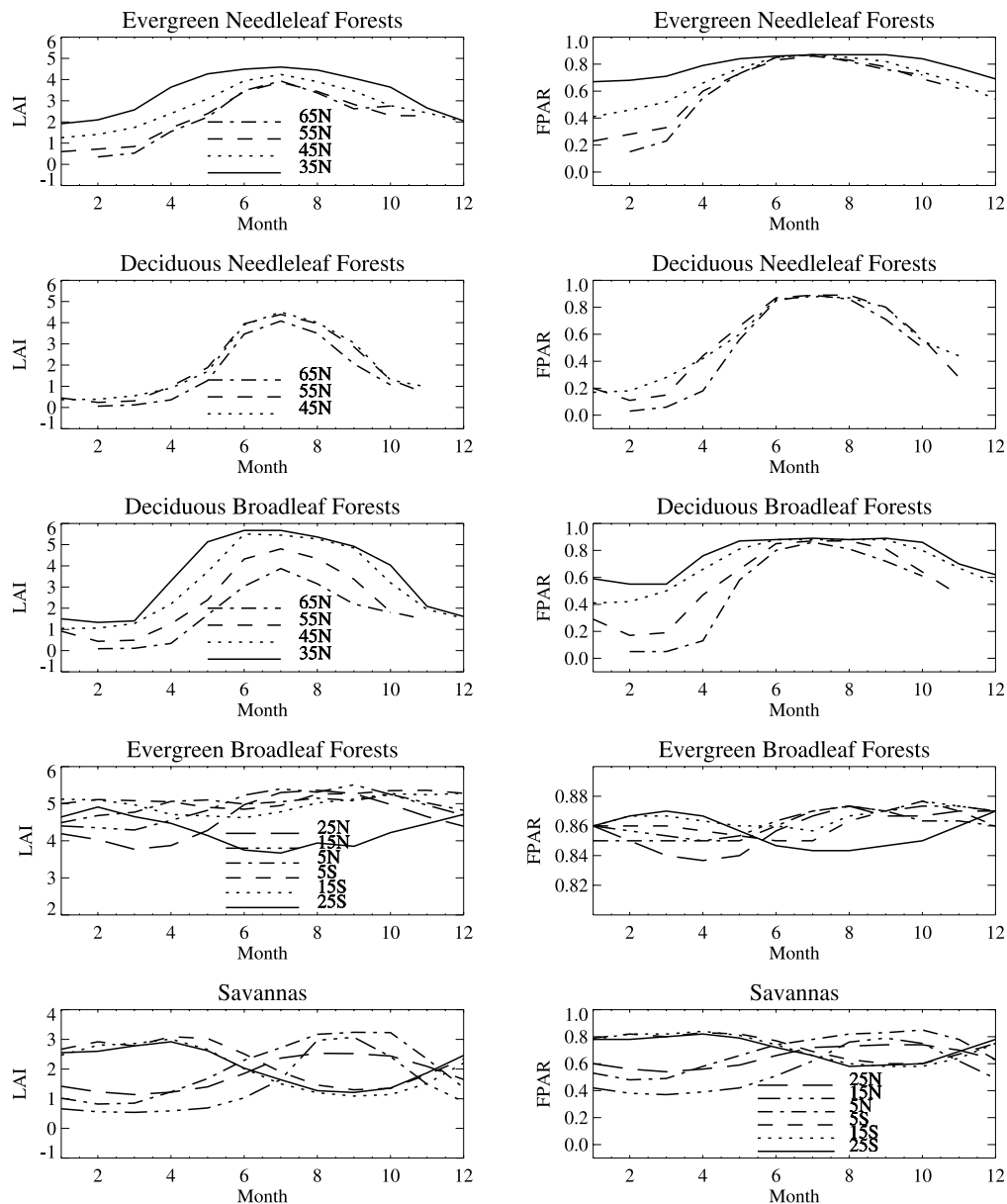


**Figure 5.** Seasonal variations of MODIS LAI and FPAR over several  $10^\circ$ -latitude bands for evergreen needleleaf forests, deciduous needleleaf forests, deciduous broadleaf forests, evergreen broadleaf forests, and savannas. Some data are not available during high-latitude winter months.

latitude ( $20^\circ$ – $50^\circ$ N,  $130^\circ$ – $95^\circ$ W) North America. Like Figures 8 and 10, the high-latitude shrubs have a higher winter CLM FPAR, mainly due to the SAI and slightly higher LAI in CLM. Although the difference between CLM LSAI and MODIS LAI remains the same (about 1.0) in Figures 8, 10, and 11 during summer, their FPAR differences vary as explained by Figure 1. We find that most of grids with the largest positive LAI and FPAR differences in Figure 6 belong to open shrublands, the major land cover type above  $55^\circ$ N. For low-latitude shrubs, MODIS and CLM show a small LAI difference, less than 0.1, with a SAI of about 0.45 as the major contribution to the FPAR bias. Surprisingly, CLM gives lower FPAR than MODIS in summer, although its LSAI is higher by 0.3 than the MODIS LAI, contrary to the simulations in Figure 1. This

can be attributed to neglect of interactions between vegetation and the underlying soil in the scheme used in CLM (more discussion in section 5).

#### 4.2.4. Croplands

[35] A region in southeast China ( $15^\circ$ – $40^\circ$ N,  $100^\circ$ – $120^\circ$ E) is selected (Figure 12). The CLM LSAI is comparable with MODIS LAI from January to June but shows small variations after June, resulting in a similar variation in FPAR. More than 50% of the grids whose CLM LSAI and FPAR are both smaller than MODIS in the NH are crops.

#### 4.2.5. Savannas

[36] Savannas, defined as land with forest canopy cover between 10–30% and with herbaceous and other understory systems, are mostly located in tropical and subtropical regions. Here (Figure 13) we selected north Africa ( $5^\circ$ –

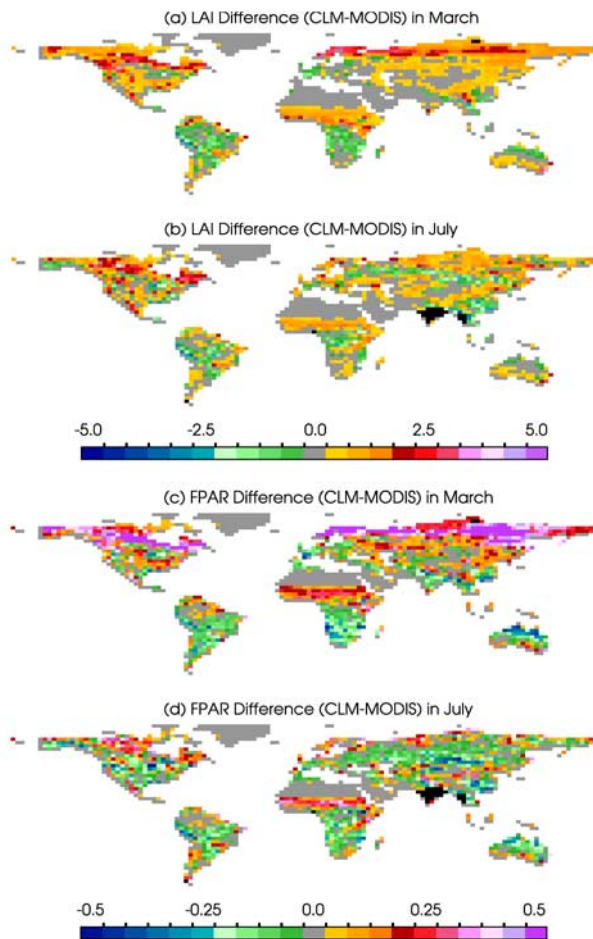


**Figure 6.** Spatial pattern of differences (CLM-MODIS) in (a) March LAI, (b) July LAI, (c) March FPAR, and (d) July FPAR. Areas in black denote no data.

15°N, 0°–40°E) and south Africa (25°–18°S, 20°–35°E). CLM and MODIS show lower values during the dry season (winter) than the wet season (summer) in both regions, with a more distinct seasonality in MODIS. The model overestimates FPAR values due to its SAI during the dry season, while it underestimates LSAI and FPAR during the wet season. Similar results are also observed for woody savanna in Africa.

#### 4.2.6. Evergreen Broadleaf Forests

[37] Two regions are shown (Figure 14). In central Africa (10°S–0°, 10°–30°E), observations are higher than those from the model. A double-peak seasonality observed in the MODIS data is consistent with local precipitation, indicating a plausible seasonal response of LAI and FPAR to precipitation. In the Amazon (10°S–0°, 70°–50°W), CLM LSAI is also smaller than the MODIS LAI. They differ by as much as 1.3 from September to December, with the smallest difference in May. The FPAR difference is very small during the whole year. MODIS has a much better seasonal cycle than CLM, but improvements are still needed when compared with the seasonal cycle of local precipitation. The ecological expectation is that LAI should remain constant with their values of dry season or peak during the wet season. Possibly, the extensive clouds during the

wet season might partially contaminate the satellite data, although improvements have been made in Collection 4 data. In addition, the MODIS LAI is much higher than the model LAI. Possibly, the low value of CLM LAI results from quality problems with the AVHRR data related with satellite changeover/drift or its lack of explicit atmospheric corrections.

## 5. Discussion

[38] The values of FPAR are mainly determined by LAI in MODIS and by LSAI in CLM. In the Northern Hemisphere winter, the model gives LSAI and FPAR values significantly higher than MODIS observations, mainly due to the model SAI. However, MODIS may give too small LAI and FPAR in the presence of snow during the winter season. As we mentioned in section 2.1, the MODIS LAI and FPAR are derived either from the main algorithm or the NDVI-based back-up algorithm. Since snow is not included in either the current background reflectance properties of the main algorithm's LUTs or the back-up algorithm, the main algorithm generally fails over snow covered pixels and the LAI values are generated with low confidence by the back-up algorithm, especially for northern high-latitude needleleaf forests (W. Yang et al., Analysis of MODIS LAI and FPAR collections 1 and 3 data set time series from July 2000 to December 2002, submitted to *Remote Sensing of Environment*, 2003).

[39] Although this paper has attempted to exclude snow covered pixels from our data processing, some may still contain a small fraction of snow or be contaminated by adjacent snow covered pixels. The current MODIS data uses normalized snow difference indices [Hall et al., 2002] to assess the presence of snow when a threshold value is exceeded. This method, for example, may label dense vegetation partially covered or underlain by snow as snow free. The presence of snow will influence both the NDVI-LAI relationship and single-scattering albedo and thus degrade the accuracy of LAI-FPAR retrievals in the MODIS algorithm.

[40] To better discuss this issue, we simulate the NDVI-LAI relationship (Figure 15) under snow-free and snow-present conditions at SZA = 70° in CLM. For simplicity, here the CLM rather than the MODIS algorithm is used. NDVI values are calculated from the two broadband albedos. We assume that snow albedo is 0.7 in VIS and 0.4 in the near-infrared band (0.7–5.0 μm), and that snow depth (SD) is allowed to vary from 0.1 to 1.1 m, which results in the fraction of snow covered soil (vegetation) ranging from 50% to 91% (1% to 9.9%). Without snow, CLM NDVI is less than 0.3 for LAI = 0, and it would be reasonable to assume that a pixel is bare soil (LAI = 0) if its NDVI is less than 0.1, as assumed in the MODIS algorithm. When snow is present, LAI could be as high as 0.55 when NDVI is as low as about 0.1. Snow significantly decreases the satellite measured NDVI in high latitudes from October to April when it covers most of the area. Since there are no LUTs for snow covered surface reflectances, the MODIS algorithm may use snow-free LUTs to retrieve LAI in the presence of snow and therefore underestimate LAI (assigning zero for pixels with NDVI less than 0.1).

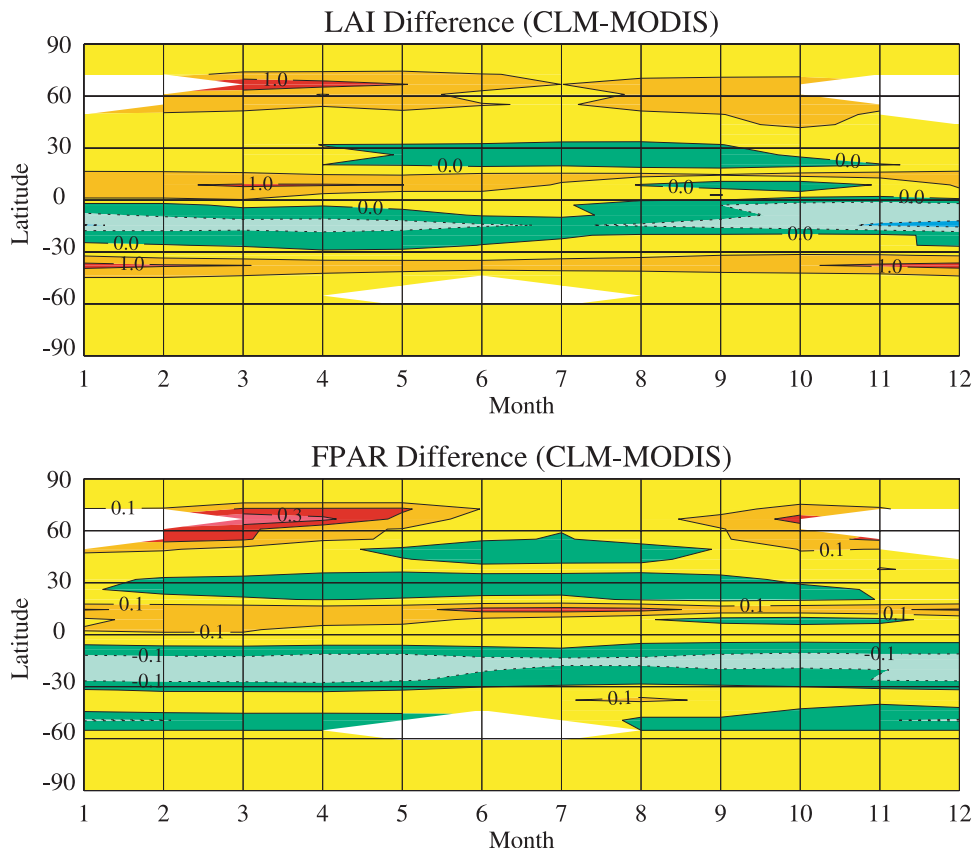


**Figure 7.** Spatiotemporal variations of differences (CLM-MODIS) in LAI and FPAR. Areas in white denote no data available during high-latitude winter months.

[41] In addition, snow and ice frozen on leaves may also significantly alter the leaf single-scattering albedo and thus increase variations of vegetation reflectance (Y. Knyazikhin, personal communication). For a given biome type, MODIS assumes that variations in the single-scattering albedo do not exceed 10%. This assumption may not be met under winter conditions. Improvement of winter LAI retrievals from optical remote sensing requires accurate specification of the single-scattering albedo, which should be a weighted sum of leaf and ice albedos. For this, additional information

about the presence of ice, its amount and optical properties are needed.

[42] This paper highlights the importance about how to better represent the effects of nongreen canopy surfaces such as stems and dead leaves through SAI in the model. Comparisons between CLM and MODIS albedo [Zhou *et al.*, 2003] also find large discrepancies for late winter conditions due to the presence of SAI in CLM. CLM treats LAI and SAI the same in FPAR and albedo parameterizations, making the contribution of SAI to albedo and

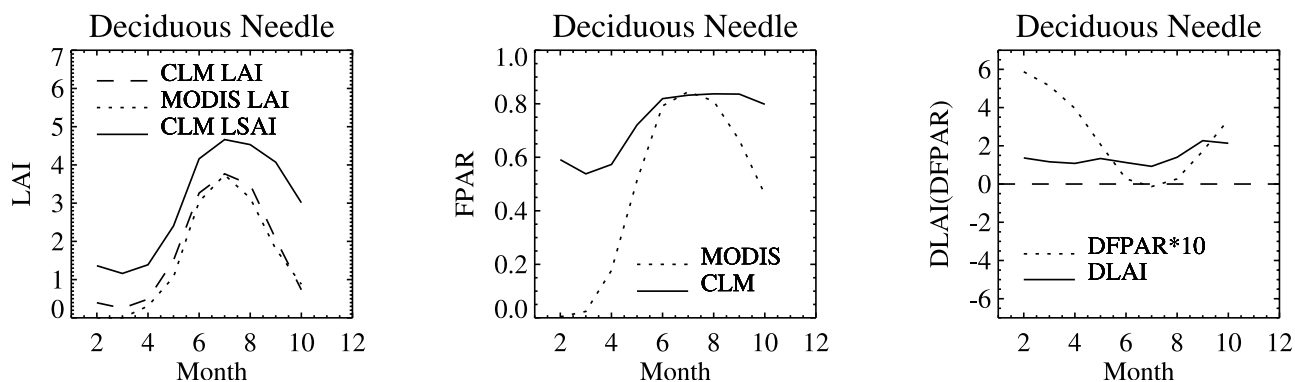


**Figure 8.** Seasonal variations of CLM LSAI, LAI, and FPAR, MODIS LAI and FPAR, and their differences ( $DLAI = LSAI_{CLM} - LAI_{MODIS}$ ;  $DFPAR = FPAR_{CLM} - FPAR_{MODIS}$ ) for deciduous needleleaf forests in Siberia ( $50^{\circ} - 65^{\circ}N$ ,  $100^{\circ} - 140^{\circ}E$ ). Some data are not available during high-latitude winter months.

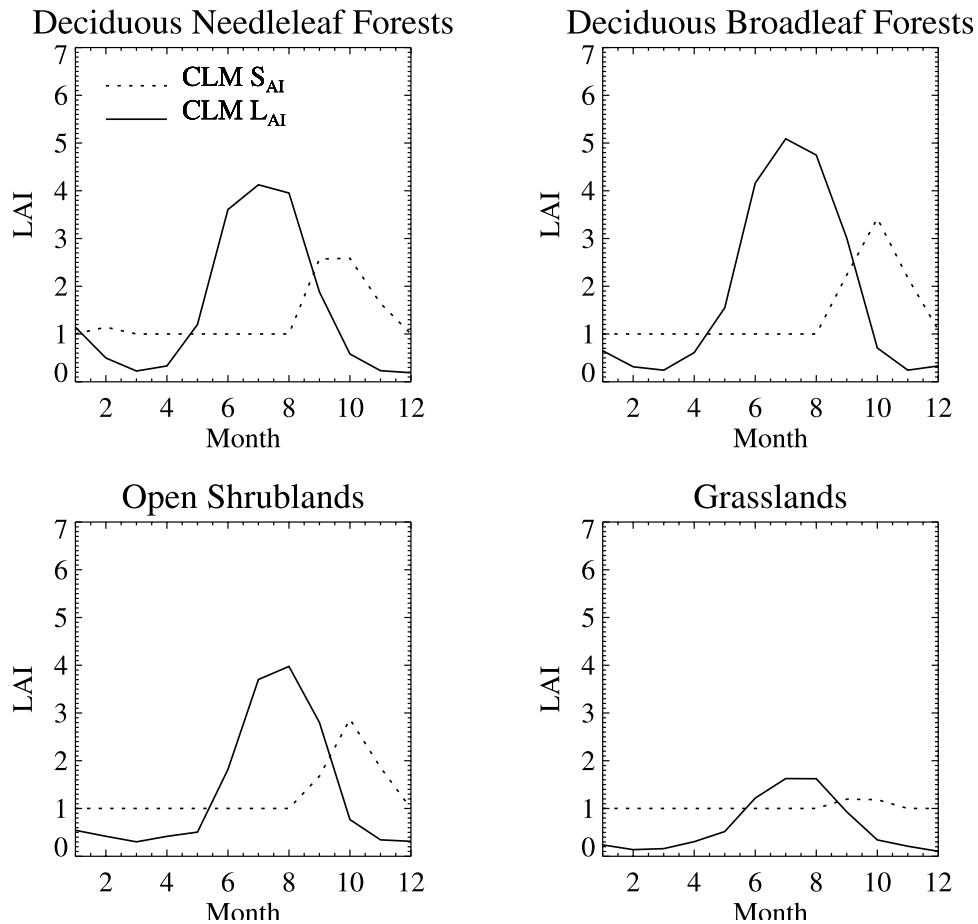


**Figure 9.** Seasonal variations of  $L_{AI}$  and  $L_{SAI}$  used in CLM (with respect to vegetated area) in  $50^{\circ}$ – $59^{\circ}$ N for four deciduous vegetation types: deciduous needleleaf forests, deciduous broadleaf forests, open shrublands, and grasslands.

FPAR much larger than that of LAI in winter. In addition, single-scattering albedo is different between stems and green leaves. Therefore the role of SAI in FPAR and albedo parameterizations needs reformulation. How to use MODIS surface reflectances to estimate SAI is another interesting question.

[43] A related issue is the different conceptualization of FPAR in MODIS and CLM. The MODIS algorithm for

LAI and FPAR determines a FPAR only from the contribution of green leaves, while the model assumes FPAR should also include that absorbed by stems. Alternatively, in support of estimates of transpiration and carbon assimilation, it may be better to include, as observed, only the green leaf contribution. Since nongreen surfaces exist in canopies, their role needs clarification both in model treatments and in the context of the MODIS data. These

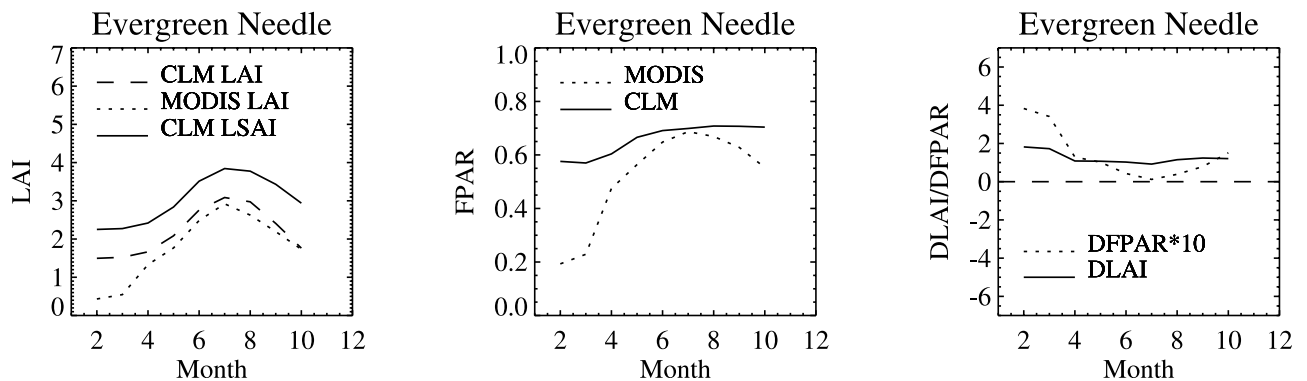


**Figure 10.** Same as Figure 8 but for evergreen needleleaf forests in North America ( $40^{\circ}$ – $60^{\circ}$ N,  $130^{\circ}$ – $60^{\circ}$ W).

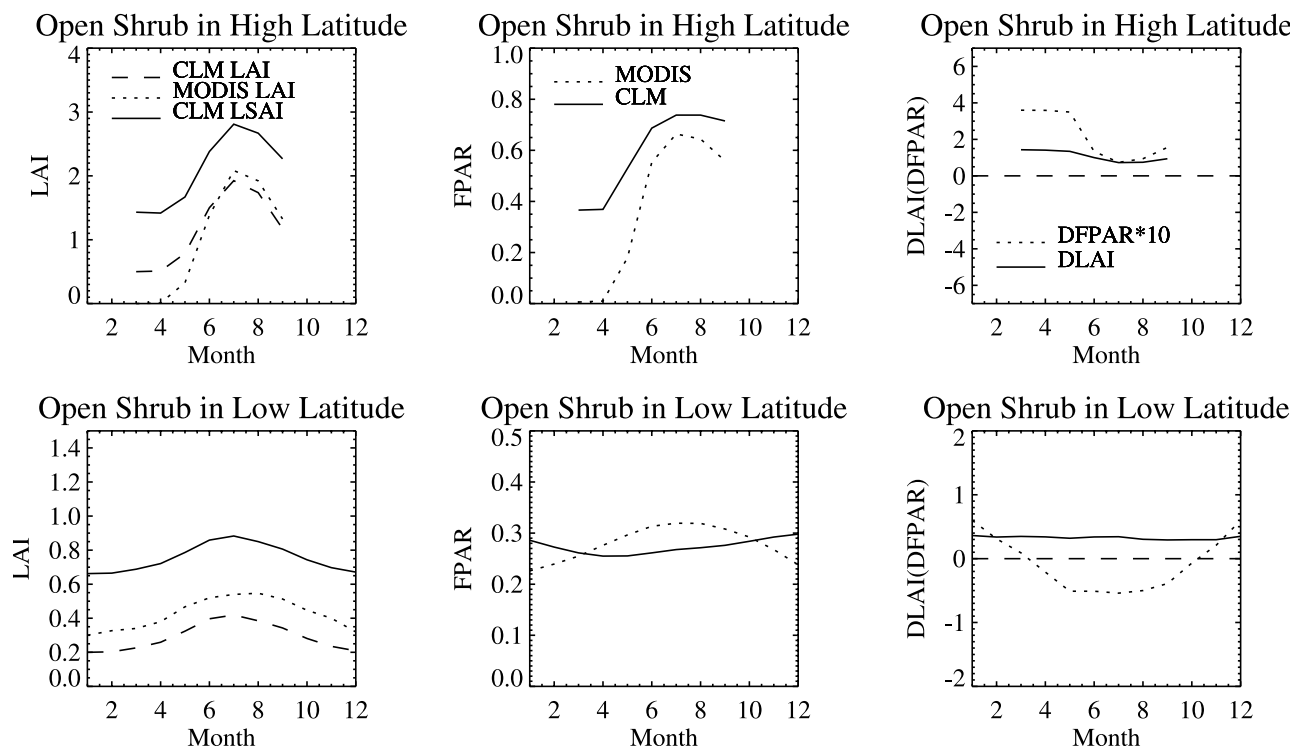


**Figure 11.** Same as Figure 8 but for open shrublands in high latitude (55°–70°N, 170°W–170°E) and low latitude (20°–50°N, 130°–95°W).

surfaces contribute to the absorption and reflection of solar radiation, and since they have larger reflectances at 858 than 648 nm, in principle they contribute to the greenness signal. However, this difference should be quite smaller for a bare canopy than a green one. Green leaves tend to cover or shade nongreen surfaces; therefore the nongreen surface contributions to estimates of FPAR may be negligible as assumed up to now by the MODIS algorithm. However, as demonstrated in our studies, these surfaces can make major contributions to a climate model’s land surface absorption of solar radiation in the absence of leaves and thus must be understood to achieve better land models.

[44] For short vegetation with bright underlying surface such as shrubs, grasses, and crops, the negative FPAR difference that is accompanied by the positive LAI difference (Figure 6) could be partially attributed to neglect of

interactions between vegetation and the underlying soil in the scheme (equation (4)) used in CLM. Such neglect could result in a negative FPAR bias as observed in northern middle latitude arid and semiarid regions (Figure 6). To estimate such effect, we calculate FPAR using both CLM scheme and the MODIS algorithm by allowing the canopy underlying soil albedo changing from 0 to 0.23 (Figure 16). Evidently, FPAR is significantly underestimated by the model scheme compared with the MODIS algorithm, which is assumed to be correct. Such underestimation is especially significant for dry soil under LAI = 1.1. For example, of the 100 grids, whose CLM LSAI is 10% higher and FPAR is 10% lower than MODIS data, 92 are classified as short vegetation types with bright underlying surface. Their mean LSAI is 1.19, and their FPAR difference between CLM and MODIS is about −0.08, consistent with Figure 16.

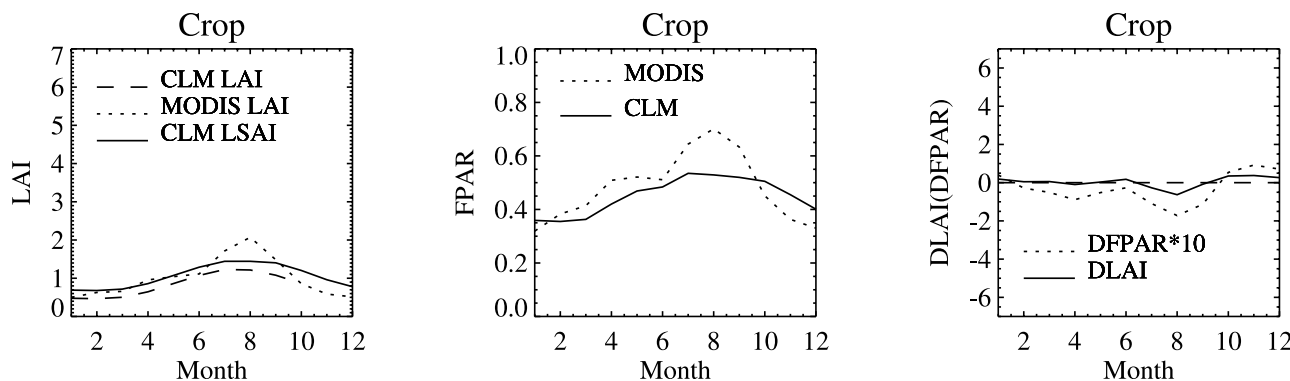


**Figure 12.** Same as Figure 8 but for croplands in China (15°–40°N, 100°–120°E).

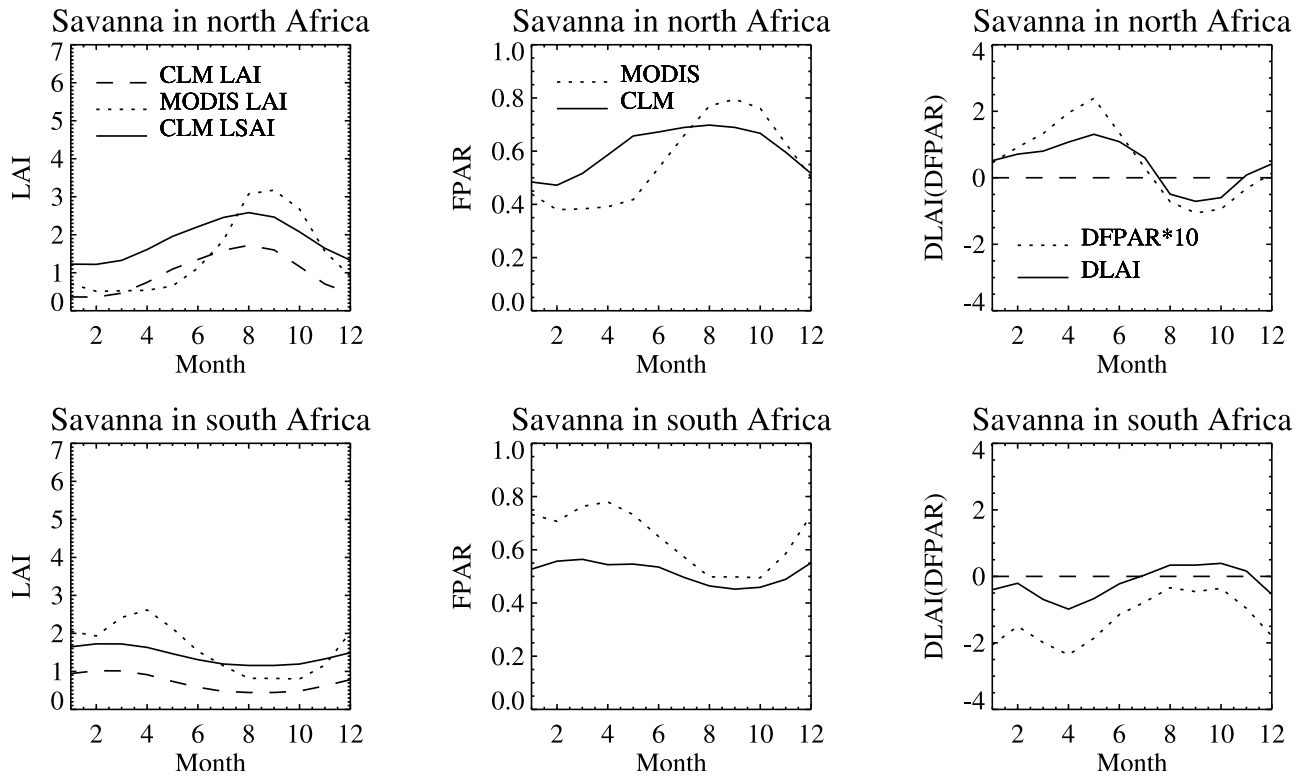


**Figure 13.** Same as Figure 8 but for savanna in North Africa ( $5^{\circ}$ – $15^{\circ}$ N,  $0^{\circ}$ – $40^{\circ}$ E) and South Africa ( $25^{\circ}$ – $18^{\circ}$ S,  $20^{\circ}$ – $35^{\circ}$ E).

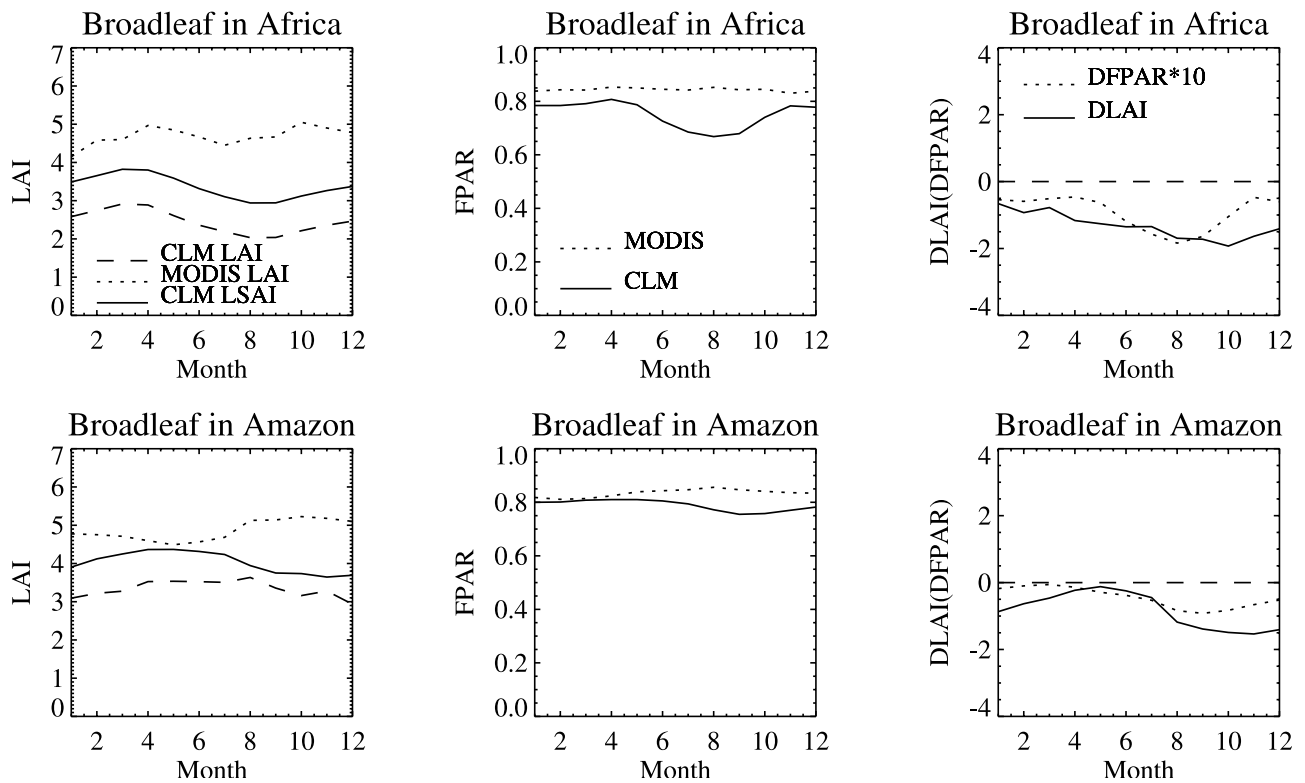


**Figure 14.** Same as Figure 8 but for evergreen broadleaf forests in Africa ( $10^{\circ}$ S– $0^{\circ}$ ,  $10^{\circ}$ – $30^{\circ}$ E) and Amazon ( $10^{\circ}$ S– $0^{\circ}$ ,  $70^{\circ}$ – $50^{\circ}$ W).

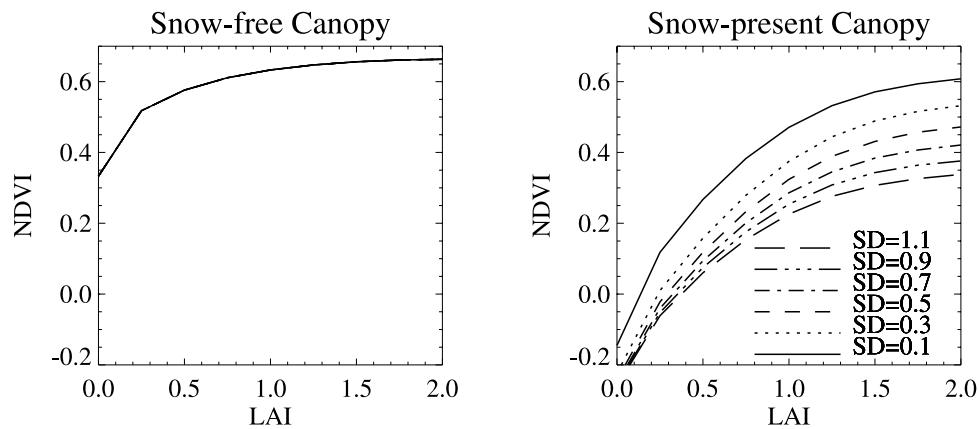


**Figure 15.** Simulated NDVI-LAI relationship under snow-free and snow-present conditions at SZA =  $70^\circ$  in CLM. Snow albedo is set as 0.7 in visible and 0.4 in near-infrared and snow depth (SD) varies from 0.1 to 1.1 m.

[45] FDIR is a very important variable in calculating FPAR and hence net primary productivity [Chameides *et al.*, 1999; Roderick *et al.*, 2001; Cohan *et al.*, 2002]. Changes in atmospheric conditions such as aerosols and clouds affect FDIR and thus FPAR. MODIS assumes that the incident solar radiation, hence FPAR, is all from direct beam. This assumption, together with limitations of atmospheric corrections used in MODIS data, may produce some uncertainties in the MODIS FPAR associated with changes in FDIR. In the model an inadequate characterization of aerosols, i.e., the aerosols are assumed to be globally homogeneous and purely scattering, may also introduce uncertainties to FPAR. Limited global aerosol observational data obscures the assessment of the relative contributions to FPAR from FDIR versus LAI. Therefore variations of FPAR from changes in FDIR in the model and MODIS are not addressed further. With the development of global AERONET and the forthcoming information about FDIR from Multiangle Imaging SpectroRadiometer (MISR) on board TERRA, this issue should be more readily investigated.

[46] Part of the LAI-FPAR bias could be also related to differences or uncertainties in specification of soil albedo and vegetation parameters such as fractional vegetation cover, which is used to produce model  $L_{AI}$  in MODIS and CLM. Interannual variations of LAI and FPAR may also contribute since only 2.5 years of MODIS data were used while 10 years of AVHRR data were used in CLM. In addition, differences in soil moisture between model and reality could account for some observed differences. The quantification of these effects, however, is still a challenge due to limited observations. However, MODIS is believed to be more reliable due to more spectral bands and higher quality than AVHRR.

## 6. Conclusions

[47] This paper compares MODIS LAI and FPAR retrievals in 2000, 2001, and 2002 with those from the Common Land Model (CLM) [Zeng *et al.*, 2002; Dai *et al.*, 2003]. Their seasonal and spatial variations are compared and the differences between the model and MODIS are investigated.

The FPAR value is mainly determined by LAI in MODIS and by leaf and stem area index (LSAI) in CLM.

[48] On average, the model underestimates FPAR in the Southern Hemisphere and overestimates FPAR over most areas in the Northern Hemisphere than MODIS observations during all seasons except northern middle latitude summer. Such overestimation is significant in winter over northern high latitudes. The MODIS LAI is generally consistent with the model during the snow-free periods but may be underestimated in the presence of snow, especially for evergreen trees. The positive FPAR bias is mainly attributed to CLM stem area index (SAI) of deciduous canopy and higher LAI than MODIS for evergreen canopy as well. The negative FPAR bias results from several factors including differences in LAI and soil albedo between CLM and MODIS or limitations of the geometric optics scheme used in the model.

[49] Therefore the MODIS algorithm needs to better represent the winter LAI retrievals and constrain with the surface observations as much as possible while the model needs to better quantify LAI and SAI. Since stems will not have the same single-scattering albedo as green

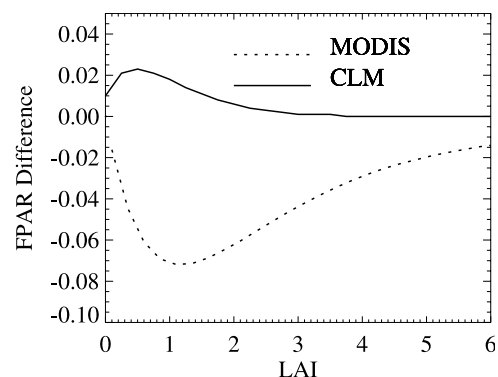


**Figure 16.** FPAR differences ( $FPAR_{\alpha_g=0.0} - FPAR_{\alpha_g=0.23}$ ) simulated from equation (2) and the MODIS FPAR algorithm with the canopy underlying soil albedo changing from 0 to 0.23 at SZA =  $30^\circ$ . Note  $FPAR_{\alpha_g=0.0}$  is assumed to be equal in both CLM and MODIS.

leaves, it may be inappropriate for the model to treat LAI and SAI the same in its FPAR and albedo parameterizations, and the role of SAI in these parameterizations needs reformulation.

[50] **Acknowledgments.** This work is funded by the NASA EOS/IDS Program (NAG5-8880).

## References

- Bonan, G. B. (1996), A land surface model (LSM version 1.0) for ecological, hydrological, and atmospheric studies: Technical descriptions and user guide, *Tech. Note NCAR/TN-417+STR*, 150 pp., Natl. Cent. Atmos. Res., Boulder, Colo.
- Bonan, G. B. (1998), The land surface climatology of the NCAR land surface model (LSM 1.0) coupled to the NCAR Community Climate Model (CCM3), *J. Clim.*, *11*, 1307–1326.
- Buermann, B., J. Dong, X. Zeng, R. B. Myneni, and R. E. Dickinson (2001), Evaluation of the utility of satellite-based vegetation leaf area index data for climate simulations, *J. Clim.*, *14*, 3536–3550.
- Chameides, W. L., et al. (1999), A case study of the effect of atmospheric aerosols and regional haze on agriculture: An opportunity to enhance crop yields in China through emission controls?, *Proc. Natl. Acad. Sci. U. S. A.*, *96*, 13,626–13,633.
- Chen, J. M., and J. Cihlar (1996), Retrieving leaf area index of boreal conifer forests using Landsat TM images, *Remote Sens. Environ.*, *55*, 153–162.
- Cohan, D. S., J. Xu, R. Greenwald, M. H. Bergin, and W. L. Chameides (2002), Impact of atmospheric aerosol light scattering and absorption on terrestrial net primary productivity, *Global Biogeochem. Cycles*, *16*(4), 1090, doi:10.1029/2001GB001441.
- Dai, Y., et al. (2003), The Common Land Model (CLM) version 1.0, *Bull. Am. Meteorol. Soc.*, *84*, 1013–1023.
- Dickinson, R. E. (1983), Land surface processes and climate-surface albedos and energy balance, *Adv. Geophys.*, *25*, 305–353.
- Dickinson, R. E., A. Henderson-Sellers, and P. J. Kennedy (1993), Biosphere-Atmosphere Transfer Scheme (BATS) version 1e as coupled to the NCAR Community Model, *Tech. Note NCAR/TN-387+STR*, 72 pp., Natl. Cent. Atmos. Res., Boulder, Colo.
- Friedl, M. A., et al. (2002), Global land cover from MODIS: Algorithms and early results, *Remote Sens. Environ.*, *83*, 287–302.
- Hall, D. K., R. A. Riggs, V. V. Salomonson, N. E. DiGirolamo, and K. J. Bayr (2002), MODIS snow-cover products, *Remote Sens. Environ.*, *83*, 181–194.
- Henderson-Sellers, A., and M. F. Wilson (1983), Surface albedo data for climate modeling, *Rev. Geophys.*, *21*, 1743–1778.
- Kiehl, J., J. Hack, G. B. Bonan, B. Bonville, D. L. Williamson, and P. J. Rasch (1998), The National Center for Atmospheric Research Community Climate Model: CCM3, *J. Clim.*, *11*, 1131–1149.
- Knyazikhin, Y., J. V. Martonchik, R. B. Myneni, D. J. Diner, and S. W. Running (1998a), Synergistic algorithm for estimating vegetation canopy leaf area index and fraction of absorbed photosynthetically active radiation from MODIS and MISR data, *J. Geophys. Res.*, *103*, 32,257–32,275.
- Knyazikhin, Y., J. V. Martonchik, D. J. Diner, R. B. Myneni, M. M. Verstraete, B. Pinty, and N. Gobron (1998b), Estimation of vegetation canopy leaf area index and fraction of absorbed photosynthetically active radiation from atmosphere-corrected MISR data, *J. Geophys. Res.*, *103*, 32,239–32,256.
- Myneni, R. B., R. R. Nemani, and S. W. Running (1997), Estimation of global leaf area index and absorbed par using radiative transfer models, *IEEE Trans. Geosci. Remote Sens.*, *35*, 1380–1393.
- Myneni, R. B., et al. (2002), Global products of vegetation leaf area and fraction absorbed PAR from year one of MODIS data, *Remote Sens. Environ.*, *83*, 214–231.
- Privette, J. L., R. B. Myneni, Y. Knyazikhin, M. Mukelabai, G. Roberts, Y. Tian, Y. Wang, and S. G. Leblanc (2002), Early spatial and temporal validation of MODIS LAI product in Africa, *Remote Sens. Environ.*, *83*, 232–243.
- Roderick, M. L., G. D. Farquhar, S. L. Berry, and I. R. Noble (2001), On the direct effect of clouds and atmospheric particles on the productivity and structure of vegetation, *Oecologia*, *129*, 21–30.
- Sellers, P. J., et al. (1997), Modeling the exchanges of energy, water and carbon between the continents and the atmosphere, *Science*, *275*, 502–509.
- Wiscombe, W., and S. G. Warren (1980), A model for the spectral albedo of snow, I, Pure snow, *J. Atmos. Sci.*, *37*, 2712–2733.
- Zeng, X., R. E. Dickinson, A. Walker, M. Shaikh, R. S. DeFries, and J. Qi (2000), Derivation and evaluation of global 1-km fractional vegetation cover data for land modeling, *J. Appl. Meteorol.*, *39*, 826–839.
- Zeng, X., M. Shaikh, Y. Dai, R. E. Dickinson, and R. B. Myneni (2002), Coupling of the Common Land Model to the NCAR Community Climate Model, *J. Clim.*, *14*, 1832–1854.
- Zhou, L., et al. (2003), Comparison of seasonal and spatial variations of albedos from Moderate-Resolution Imaging Spectroradiometer (MODIS) and Common Land Model, *J. Geophys. Res.*, *108*(D15), 4488, doi:10.1029/2002JD003326.

Y. Dai, R. E. Dickinson, M. Shaikh, Y. Tian, W. Wu, H. Yu, and L. Zhou, School of Earth and Atmospheric Sciences, Georgia Institute of Technology, 311 Ferst Drive, Atlanta, GA 30332, USA. (ytian@eas.gatech.edu)

M. Friedl, Y. Knyazikhin, R. B. Myneni, and X. Zhang, Department of Geography, Boston University, Boston, MA 02215, USA.

X. Zeng, Institute of Atmospheric Physics, University of Arizona, Tucson, AZ 85721, USA.